Research article

JHEP|Reports

Glisson's capsule matrix structure and function is altered in patients with cirrhosis irrespective of aetiology

Jessica Llewellyn,[1,2,†] **Caterina Fede**,[3,†] Abigail E. Loneker,[2,4] Chet S. Friday,[5] Michael W. Hast,[5] Neil D. Theise,[6] Emma E. Furth,[7] Maria Guido,[8] Carla Stecco,[3] Rebecca G. Wells[1,2,4,7,*]

[1]*Department of Gastroenterology and Hepatology, School of Medicine, University of Pennsylvania, Philadelphia, PA, USA;* [2]*Center for Engineering MechanoBiology, University of Pennsylvania, Philadelphia, PA, USA;* [3]*Department of Neuroscience, University of Padova, Padova, Italy;* [4]*Department of Bioengineering, University of Pennsylvania, Philadelphia, PA, USA;* [5]*Department of Orthopaedic Surgery, School of Medicine, University of Pennsylvania, Philadelphia, PA, USA;* [6]*Department of Pathology, New York University, School of Medicine, New York, NY, USA;* [7]*Department of Pathology and Laboratory Medicine, University of Pennsylvania, Philadelphia, PA, USA;* [8]*Department of Pathology, University of Padova, Italy*

JHEP Reports **2023.** https://doi.org/10.1016/j.jhepr.2023.100760

Background & Aims: Glisson's capsule is the interstitial connective tissue that surrounds the liver. As part of its normal physiology, it withstands significant daily changes in liver size. The pathophysiology of the capsule in disease is not well understood. The aim of this study was to characterise the changes in capsule matrix, cellular composition, and mechanical properties that occur in liver disease and to determine whether these correlate with disease severity or aetiology.
Methods: Samples from ten control patients, and six with steatosis, seven with moderate fibrosis, and 37 with cirrhosis were collected from autopsies, intraoperative biopsies, and liver explants. Matrix proteins and cell markers were assessed by staining and second harmonic generation imaging. Mechanical tensile testing was performed on a test frame.
Results: Capsule thickness was significantly increased in cirrhotic samples compared with normal controls irrespective of disease aetiology (70.12 ± 14.16 μm and 231.58 ± 21.82 μm, respectively), whereas steatosis and moderate fibrosis had no effect on thickness (90.91 ± 11.40 μm). Changes in cirrhosis included an increase in cell number (fibroblasts, vascular cells, infiltrating immune cells, and biliary epithelial cells). Key matrix components (collagens 1 and 3, hyaluronan, versican, and elastin) were all deposited in the lower capsule, although only the relative amounts per area of hyaluronan and versican were increased. Organisational features, including crimping and alignment of collagen fibres, were also altered in cirrhosis. Unexpectedly, capsules from cirrhotic livers had decreased resistance to loading compared with controls.
Conclusions: The liver capsule, similar to the parenchyma, is an active site of disease, demonstrating changes in matrix and cell composition as well as mechanical properties.
Impact and implications: We assessed the changes in composition and response to stretching of the liver outer sheath, the capsule, in human liver disease. We found an increase in key structural components and numbers of cells as well as a change in matrix organisation of the capsule during the later stages of disease. This allows the diseased capsule to stretch more under any given force, suggesting that it is less stiff than healthy tissue.

Introduction

The liver capsule, also called Glisson's capsule, is a layer of interstitial tissue that can also be classed as visceral fascia.[1–3] It surrounds the liver and is continuous with the interstitial spaces and matrix surrounding the portal triads, likely having a role in fluid exchange as well as cell migration within the hepatobiliary system.[4,5] The capsule has an important structural role, enclosing the parenchyma and protecting the liver from physical impact. Additionally, it is structured to allow daily size fluctuations, driven by changes in hepatocyte size post feeding as well as circadian regulation on the order of 34% in mice and 10–15% in humans.[6,7] To enable this variability in size, the normal liver capsule is thin, well innervated, and contains abundant elastic fibres, as is typical of visceral fascia.[1] These characteristics create a unique niche in which distinct populations of both macrophages and fibroblasts coexist under normal physiological conditions.[8]

Changes in the liver capsule in disease are yet to be well characterised, particularly in human disease. Second harmonic generation imaging (SHG) of the surface of fibrotic rat livers showed altered collagen organisation, with a denser collagen network and loss of the characteristic fibre waviness. These changes were highly dependent on severity of disease and were proposed to predict the degree of liver fibrosis.[9] Other rodent

Keywords: Liver fibrosis; Mechanics; Extracellular matrix; Collagen organisation; Visceral fascia.
Received 10 October 2022; received in revised form 14 March 2023; accepted 31 March 2023; available online 7 April 2023
† These authors contributed equally.
* Corresponding author. Address: Department of Medicine (GI), Perelman School of Medicine, University of Pennsylvania, 905 BRB II/III, 421 Curie Boulevard, Philadelphia, PA 19104-6140, USA. Tel.: +1-215-573-1860.
E-mail address: rgwells@pennmedicine.upenn.edu (R.G. Wells).

studies showed that, in addition to changes in the matrix, the capsular cell population changed, with mesothelial cells and fibroblasts migrating into the liver parenchyma and contributing to the myofibroblast population.[10,11] As a whole, this work suggested that the capsule is an active site of pathology in rodent liver fibrosis. However, the rodent liver capsule differs significantly from the human capsule. The mouse capsule is only ~1.7 $\mu m^2/\mu m$, with mesothelial cells, fibroblasts, and macrophages interspersed within a very thin layer of matrix; by contrast, the normal human capsule is 30–100 μm thick, with mesothelial cells found on the surface and fibroblasts and macrophages embedded within a rich network of matrix.[8,10]

During liver fibrosis progression, both collagen crosslinking and excessive matrix deposition lead to increasing resistance to mechanical loads, which serves as an indicator of disease severity.[12,13] Several non-invasive methods, including elastography, are used clinically to determine the stage of disease. In normal livers, the liver capsule is not visible under computed tomography or magnetic resonance imaging; however, this changes with disease,[14] suggesting the presence of macroscopic changes, potentially including mechanical changes that could provide metrics to determine disease progression. In this study, our aim was to characterise the matrix and cellular components and accompanying mechanical properties of the capsule in human liver disease and to establish whether these are dependent on the severity or aetiology of disease.

Materials and methods

Human samples

Ten control, six steatosis, seven moderate fibrosis, and 37 cirrhotic anonymised human liver samples were obtained by EEF at the University of Pennsylvania under institutional review board (IRB) protocol #831726, NDT at New York University under IRB protocol #il8-01106, and MG from the Ethical Committee of Treviso Hospital at the University of Padua under protocol #831726. Informed consent was obtained from individuals as per the requirements of the IRBs. Samples were from autopsies (controls, steatotic, and cirrhotic), intraoperative biopsies taken during gallbladder or bariatric surgery (steatosis and moderate fibrosis), metastatic colon cancer resections (uninvolved tissue as controls), and liver explants (cirrhosis). Cirrhotic samples reflected a range of disease aetiologies, including non-alcoholic fatty liver disease (NAFLD), ethanol-induced liver disease, primary sclerosing cholangitis, chronic HCV infection, heart disease, and other causes, such as autoimmune hepatitis, polycystic liver disease, hilar cholangitis, and iron overload secondary to thalassaemia. A power calculation was carried out using changes in capsule thickness from a preliminary group of patient samples. We assumed normal distribution and found a difference in means of 101 μm with a SD of 47. Six individuals per group were calculated to be required to reach a power of 0.9 and type I error probability of 0.05. Therefore, samples were collected until all groups had a minimum of six per group. Given limited numbers of sections for certain samples, a subset of randomly selected samples per group were selected for each staining. The age and sex of patients are shown in Fig. S1. All samples were reviewed blindly by NDT and EEF before being classed in one of four groups. Samples without steatosis, cell infiltration, or fibrosis were defined as controls; samples with a fat score of 1–3 and no fibrosis were defined as steatosis; samples with or without fat but a fibrosis score of 1–3 were defined as moderate fibrosis; and samples with a fibrosis score of 4 were defined as cirrhotic samples.

Histology, staining, and image analysis

Livers were cut into 1–2 cm-long pieces containing the capsule layer and the underlying parenchyma, and were formalin fixed and paraffin embedded before being sectioned at a thickness of 5 μm. Before staining, sections were deparaffinised in xylene, rehydrated in a gradient of ethanol solutions, and washed in diH_2O. Next, heat-mediated antigen retrieval was carried out in 10 mM citric acid, pH 6 before immunohistochemical staining. Further details of the staining and image analysis are provided in the Supplementary methods.

Second harmonic generation imaging

SHG imaging was carried out on fixed sections (2D) as well as on a subset of non-processed samples (3D). Fixed and paraffin-embedded sections were imaged without dewaxing/rehydration (2D). Capsules were also carefully peeled off from the surface of fresh livers before being formalin fixed and imaged (3D). All samples were imaged using a Leica SP8 confocal/multiphoton microscope and Coherent Chameleon Vision II Ti:Sapphire laser (Leica, Buffalo Grove, IL, USA) tuned to a wavelength of 910 nm and the Leica Application Suite (LAX, Deerfield, IL, USA) software. SHG of collagen generates both forward and backward signals; directionality of scatter is dependent on the size and orientation of the fibrils, with backward scatter associated with more immature fibrils.[15]

Mechanical testing

Human liver capsules were carefully peeled away from parenchyma using forceps before being frozen until use. Fresh tissue of a minimum size of 2 cm × 1 cm was required; therefore, only samples collected from cirrhotic explants and uninvolved tissue from metastatic colon cancer resections (control) could be used for this analysis. These unfixed frozen peeled capsules were defrosted and placed into 1% PBS for the duration of mechanical testing. Membrane cross-sectional area was calculated using a custom laser-based measurement device. This device uses a confocal displacement laser (CL-3000, Keyence Corporation, Ithaca, NY, USA), which has the capacity to measure transparent samples. Tensile testing was performed on a test frame (5542, Instron Inc.) equipped with a 10 N load cell. Samples were prepared on both ends using 400-grit sandpaper held in place with cyanoacrylate glue. Using custom aluminium grips, specimens underwent a tensile ramp-to-failure at a rate of 0.03 mm/s. Outcome metrics included max load (N/mm), stiffness (N/mm), max stress (MPa), max strain (mm/mm), and modulus (MPa).[16]

Statistical analysis

Statistical significance was assessed using one-way ANOVA followed by Tukey's post hoc analysis, one or two-tailed Student's *t* test, or a Pearson's correlation, calculated with Prism 9 (GraphPad Software, La Jolla, CA, USA). One-tailed Student's *t* tests were used for differences in crimping and alignment because these were hypothesised to be reduced in cirrhotic samples. A value of $p < 0.05$ was regarded as statistically significant. The tests used for each analysis are noted in the figure legends.

Results

Capsule thickness and number of cells increase in patients with liver disease

Liver capsules from controls, and from patients with steatosis, moderate fibrosis, and cirrhosis were assessed for capsule thickness and cellularity. Capsules of cirrhotic samples were noticeably thicker when assessed by H&E staining, which also demonstrated that thickening was heterogeneous within a given patient sample (Fig. 1A and B). Thickening of the capsule was dependent on severity of disease but independent of aetiology (Fig. 1A–C). Quantification of thickness showed that steatotic and moderately fibrotic samples were unchanged compared with controls; however, cirrhotic samples were ∼3.3 times thicker than controls (231.58 μm ± 21.82 and 70.12 μm ± 14.16, respectively; Fig. 1B). Additionally, capsule thickness positively correlated with parenchymal fibrosis (Fig. 1C) and portal tract thickness (Fig. 1D). Capsules from cirrhosis of different aetiologies had similar ranges of thickness and no clustering was observed. Next, the number of cells found within the capsule was counted. Control and steatotic samples had similar numbers of cells ($2.19 \times 10^{-4} \pm 2.74 \times 10^{-6}$ and $2.58 \times 10^{-4} \pm 4.76 \times 10^{-6}$nuclei/pixel, respectively); however, both moderately fibrotic and cirrhotic livers had an increased number of cells ($5.76 \times 10^{-4} \pm 7.26 \times 10^{-6}$ and $4.157 \times 10^{-4} \pm 3.47 \times 10^{-6}$ nuclei/pixel respectively) per capsule area (Fig. 1D), suggesting that an increase in cell number precedes thickening of the capsule.

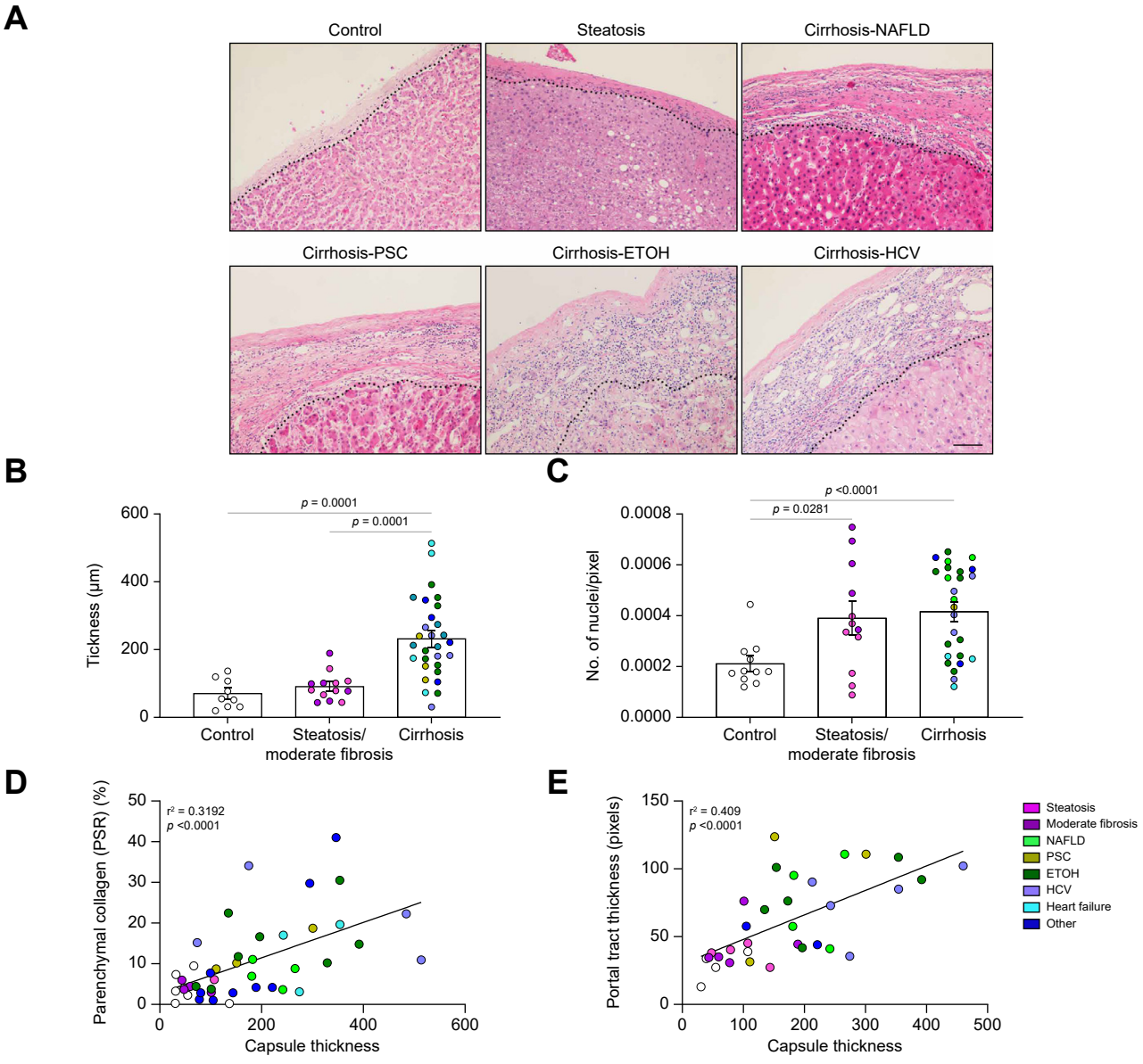

Fig. 1. Changes in liver capsules in patients with liver disease. (A) Representative H&E images of human livers with no disease (control), steatosis, and cirrhosis of different aetiologies. Capsules are found above the dotted line. (B) Quantification of liver capsule thickness. (C) Quantification of cell number in the capsule. Control *vs.* steatosis (NS), control *vs.* moderate fibrosis ($p = 0.0004$), steatosis *vs.* moderate fibrosis ($2.578 \times 10^{-4} \pm 4.76010^{-5}$ and $5.762 \times 10^{-4} \pm 7.262^{-5}$, respectively, $p = 0.0052$), moderate fibrosis *vs.* cirrhosis ($p = 0.1578$). (D) Correlation between parenchymal fibrosis (% collagen stained by Picrosirius red) and capsule thickness. (E) Correlation between portal tract collagen thickness and capsule thickness. Thickness and number of nuclei were analysed by one-way ANOVA and are shown as mean ± SEM. Correlation analysed by Pearson's correlation. N = 9–31. Scale bar: 50 μm. ETOH, ethanol-induced liver disease; NAFLD, non-alcoholic fatty liver disease; PSC, primary sclerosing cholangitis.

Increase in vascular, immune cell, fibroblast, and biliary epithelial cell populations in capsules from cirrhotic livers

To identify the cells present in the capsule, samples were stained for vascular endothelial, immune, fibroblast, and biliary epithelial cell (BEC) markers. Cirrhotic capsules were richer in vascular structures ($CD31^+$) (Fig. 2A and B) compared with control samples. The thickness of the capsule positively correlated with the number of capsular structures, suggesting a potential link between capsular angiogenesis and increase in thickness. However, no correlation was observed with increased parenchymal $CD31^+$ (Fig. 2A and B; Fig. S2A and B). There was also a large population of small circular leukocytes ($CD45^+$) in the lower layers of the capsule of cirrhotic samples (Fig. 2A and C). Macrophages ($CD68^+$) have previously been shown to be present in human capsule.[8] Here, we showed that they comprised ~10% of the liver capsule cell population in all groups (Fig. 2A and D); the absolute number of macrophages increased with disease, although their proportion within the overall cell population remained constant.

Fibroblasts, identified by vimentin staining, were found in all groups (Fig. 2A); however, activated fibroblasts (αSMA^+) were significantly increased only in cirrhotic samples (Fig. 3A and B). BECs and mesothelial cells were stained using keratin 7 (K7) and 19 (K19) (Fig. 3A and C). Mesothelial cells were found (but not consistently) on the surface of the liver capsule of all sample groups. This was confirmed by calretinin staining (Fig. S3), in which few, if any, calretinin-positive cells were observed within the capsule. However, several could be seen detaching from the surface, suggesting that the lack of mesothelial cells on the surface of our samples is an artefact of tissue handling. BECs (positive for K7 and K19 and negative for calretinin) were found in lower layers of the capsule, often at the interface with the parenchyma. These were organised in ductal structures as well as being present as individual cells and were most significantly increased in patients with cirrhosis (Fig. 3C). To determine whether cell proliferation contributed to the observed increase in cells, capsules were stained with Ki67, a nuclear protein marker for cellular proliferation. Overall, there was no change in proliferation observed in the disease groups compared with controls (Fig. 3D; Fig. S4).

Collagen fibres and organisation are altered in patients with liver cirrhosis

Collagen fibres and organisation were visualised by SHG microscopy (Fig. 4). There appeared to be two layers (the upper 70 μm and the remaining lower layer), and the content of collagen was quantified in each. The percentage area of collagen was consistent for the top layer for all disease states; however, capsules from cirrhotic samples had significantly less dense collagen in the lower layer (Fig. 4A and B). We calculated the uniformity index (which quantifies the regularity of collagen fibres) from 2D SHG images and found that collagen fibres in control and steatotic/moderately fibrotic samples were distributed in a relatively

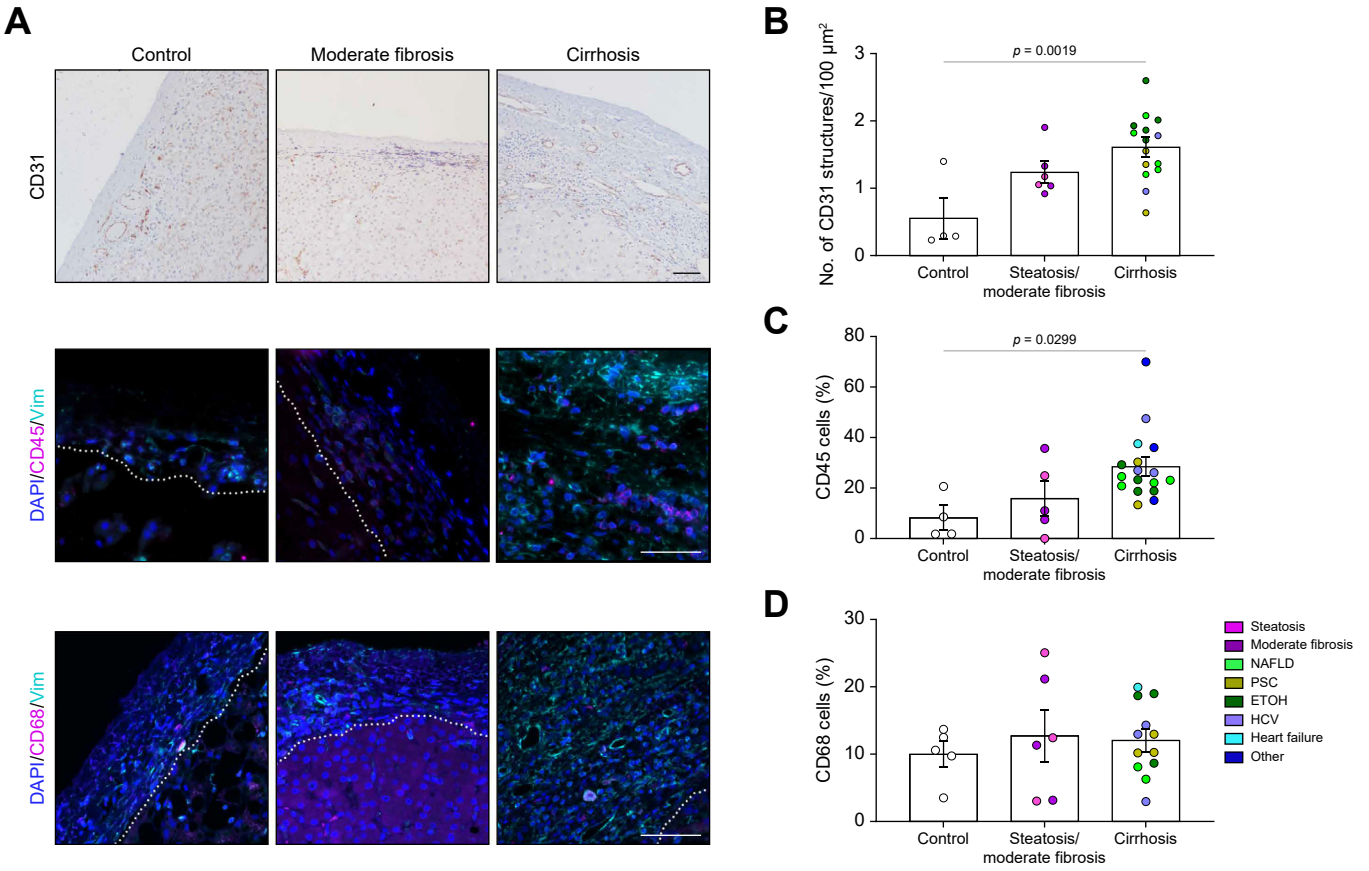

Fig. 2. Increase in vascular and immune cells. (A) Representative images of control, moderately fibrotic, and cirrhotic samples (NAFLD in this example) stained for CD31 (vascular endothelial cells; brown), DAPI (nuclei; blue), CD45 (leucocytes; pink), CD68 (macrophages; pink), or vimentin (fibroblasts; teal). Capsule found above dotted line. (B) Quantification of the number of CD31-positive structures. (C) Quantification of CD45-positive cells in the capsule. (D) Quantification of CD68-positive cells in the capsule. Data were analysed by one-way ANOVA and are shown as mean ± SEM. N = 4–17. Scale bars: 50 μm. ETOH, ethanol-induced liver disease; NAFLD, non-alcoholic fatty liver disease; PSC, primary sclerosing cholangitis.

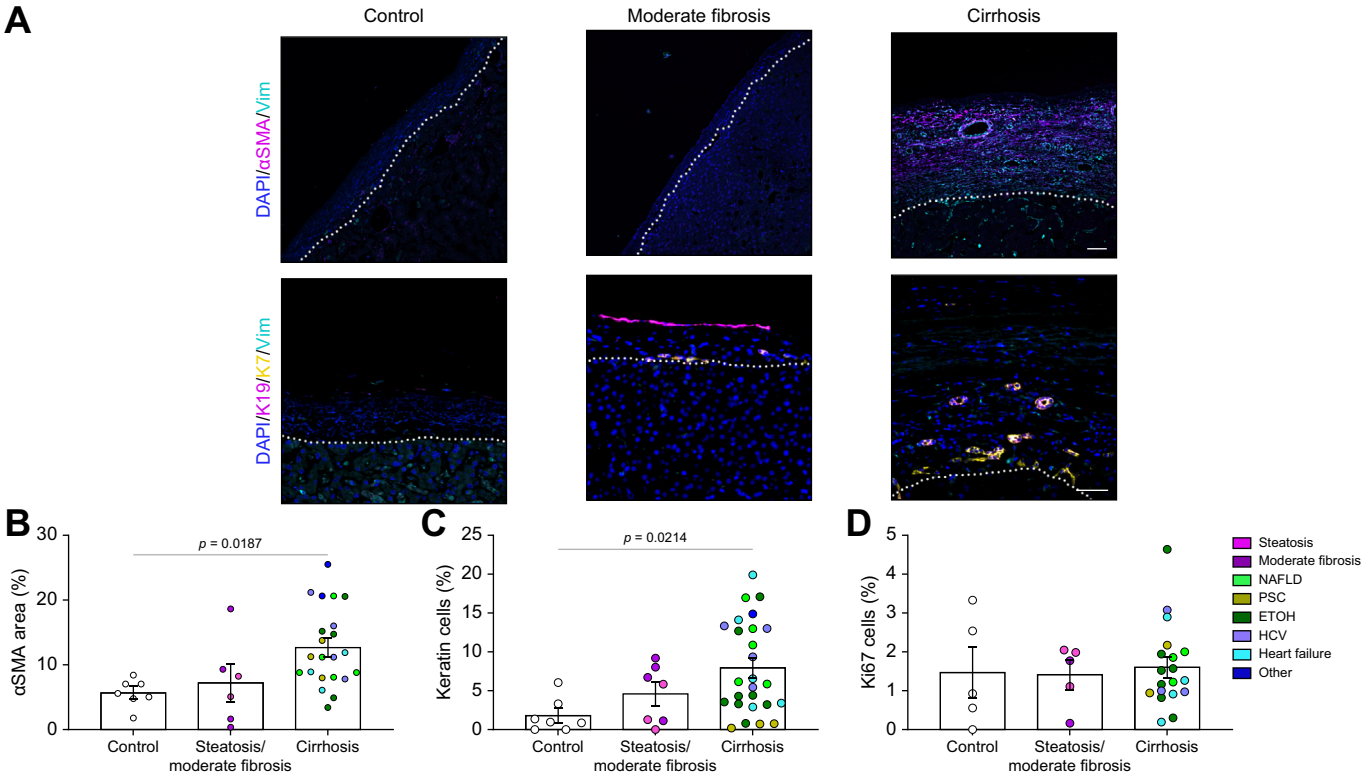

Fig. 3. Increase in fibroblasts and biliary epithelial cells in diseased capsule. (A) Representative images of control, moderately fibrotic, and cirrhotic samples (NAFLD in this example) stained for DAPI (nucleus; blue), vimentin (fibroblasts; teal), αSMA (activated fibroblasts; pink), K19 and K7 (biliary epithelial cells, pink and yellow respectively). Capsule found above dotted line. (B) Quantification of αSMA percentage area. (C) Quantification of keratin-positive cells in the capsule. (D) Quantification of Ki67-positive cells in the capsule. Data were analysed by one-way ANOVA and are shown as mean ± SEM. N = 5–24. Scale bars: 50 μm. ETOH, ethanol-induced liver disease; HA, hyaluronic acid; NAFLD, non-alcoholic fatty liver disease; PSC, primary sclerosing cholangitis; SMA, smooth muscle actin.

uniform manner, whereas collagen fibres in cirrhotic capsules were more irregular (Fig. 4A and C).

To further understand the organisation of collagen in the capsule, 3D top-down SHG imaging was performed on freshly fixed samples (Fig. 4D). Individual collagen fibres in control samples had a characteristic crimp, which is often found in healthy tissue[17] and which provides low levels of absorption and compliance. Collagen fibres in cirrhotic samples largely lost this crimp, although bundling of fibres, as assessed by SHG imaging, appeared unaffected (Fig. 4D and E; Fig. S5). Collagen fibres in controls were organised in highly aligned sheets layered perpendicularly on top of each other, creating a 3D cross hatch pattern that has also been described as a 'two fibre family' organisation.[18] This was quantified using a previously described method,[19] which assigns fibres to directional families, clearly showing that, in most cases, two individual directional families alternate in contributing to each layer of the collagen network (Fig. S6). The alignment index, which measures how aligned fibres are within these assigned families, was reduced, suggesting that overall organisation is disrupted in capsules from cirrhotic livers (Fig. 4D and F).

Extracellular matrix composition of liver capsule is altered in patients with liver cirrhosis

Liver fibrosis leads to the excessive deposition of a complex network of structural and biochemically active matrix proteins in the liver parenchyma that, in turn, help drive progression of disease. However, the extracellular matrix composition (ECM) composition of the capsule and how this changes in disease are unclear. We used immunostaining to define changes in matrix composition. We found layers of thick elastic fibres, important for capsule stretch and recoil during fluctuations in liver size, in the control samples. Scattered hyaluronic acid (HA) was also identified in the lower layer of the healthy capsule. Collagen 3, important for collagen fibrillogenesis as well as repair and regeneration of tissues,[20] was also found in relatively abundant amounts throughout the capsule. Versican, a proteoglycan, was found in limited amounts. Capsules from steatotic and moderately fibrotic livers showed similar distributions of these matrix components (Fig. 5A–E). In cirrhosis, elastic fibres and collagen 3 were increased but in proportion to the increase in thickness, leading to a similar overall concentration (% area) and collagen 1:3 ratio as in controls (Fig. 5B and D; Fig. S7). Both HA (control 13.52 ± 5.261% *vs.* cirrhosis 35.99 ± 3.505%) and versican (control 0.6797 ± 0.4168% *vs.* cirrhosis 17.50 ± 3.010%) were significantly increased, primarily in the lower capsule at the interface with the parenchyma (Fig. 5A, C, and E).

Cirrhotic liver capsule is less resistant to mechanical load

To establish whether the observed changes in the composition and organisation of the capsular matrix affect its function, we tested capsule mechanical properties. Cross-sectional areas of peeled capsules were measured and specimens were placed on a test frame (Fig. 6A), where force–displacement profiles were recorded (Fig. 6B). Several mechanical properties of interest were calculated, including stiffness (N/mm), which is the slope of the force–displacement curve. Additionally, stress, which is the amount of force exerted on the tissue divided by cross-sectional

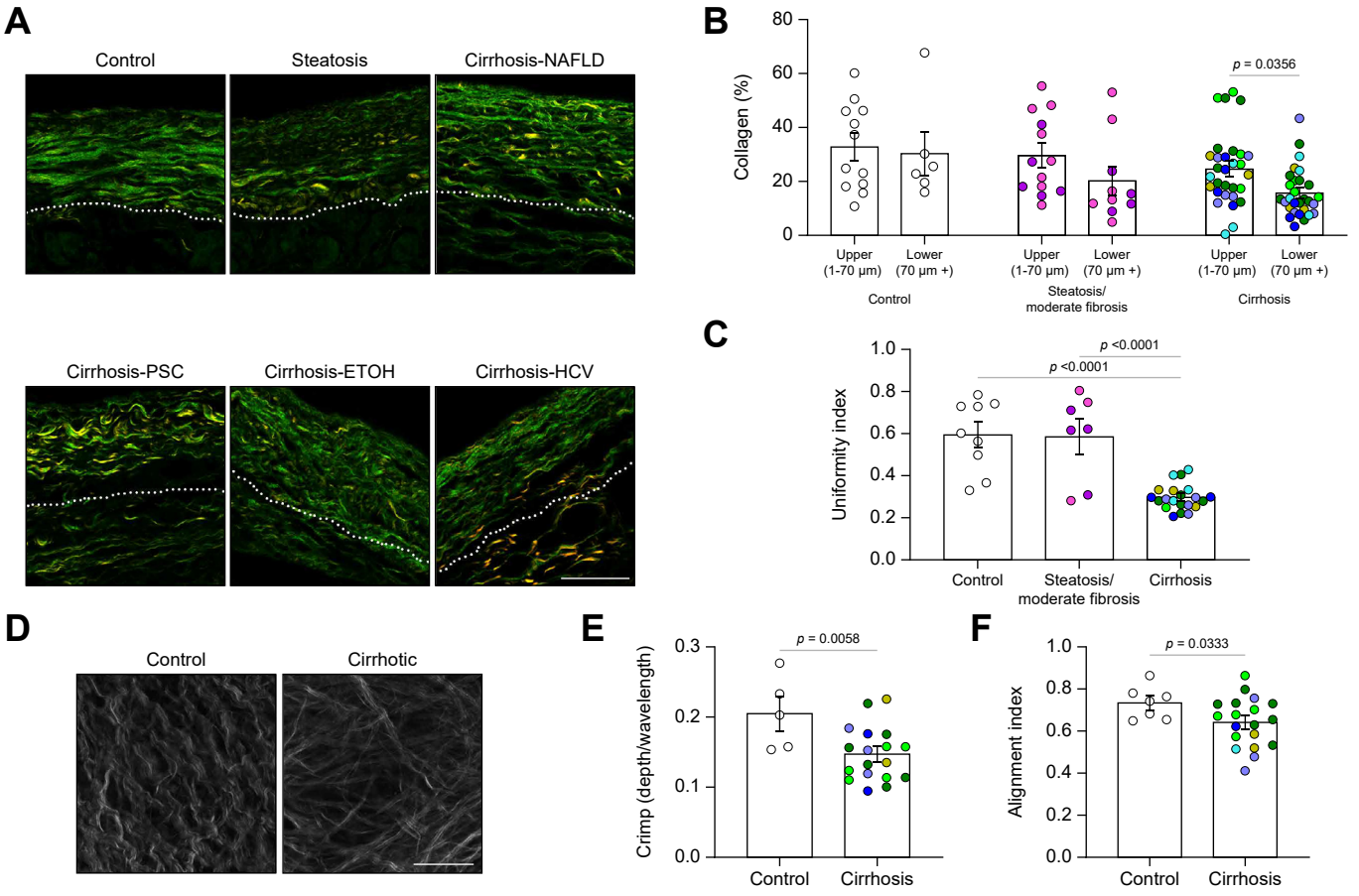

Fig. 4. Organisation of the capsular collagen network is disrupted in cirrhosis. (A) Representative second harmonic generation (SHG) images of cross-sections of control, steatotic, or cirrhotic samples. Dotted line demarcates the upper layer (1–70 μm from surface) and lower layer (70 μm+) of the capsule. (B) Quantification of percentage area of collagen in the different layers of the capsule. N = 12–31. (C) Calculated uniformity index. N = 7–20. Data were analysed by one-way ANOVA and are shown as mean ± SEM. (D) Representative top-down SHG images of a control and a cirrhotic sample. (E) Calculated collagen fibre crimp. (F) Calculated alignment index of collagen fibres. Data analysed with an unpaired one-tailed Student's *t* test and shown as mean ± SEM. N = 5–18. Scale bars: 50 μm. ETOH, ethanol-induced liver disease; NAFLD, non-alcoholic fatty liver disease; PSC, primary sclerosing cholangitis.

area, and strain, which is the amount of displacement of the tissue relative to its initial length, were calculated. Normalised measures of strength were calculated from the stress–strain curve, including the elastic modulus (MPa), which is the slope of the stress–strain curve. Clear clustering of control and cirrhotic capsules were seen (Fig. 6C), suggesting altered mechanics in disease. The liver capsule has biphasic mechanics, with an initial linear phase at low strain (0–7%) and a second linear phase at higher strain (10–30%).[21,22] Unexpectedly, cirrhotic capsules required less force and stress to fail compared with controls (Fig. 6D and E), and had decreased moduli (Fig. 6F; Fig. S8B). The moduli of cirrhotic capsules were significantly less compared with control capsules in both the toe region (low strains; cirrhotic 13.42 ± 2.61 Mpa and control 34.11 ± 11.92 MPa, respectively) and the elastic region (high strains; cirrhotic 38.04 ± 9.47 MPa and control 123.9 ± 11.63 MPa) (Fig. 6F; Fig. S8C).

Discussion

The contribution of the capsule to the pathogenesis of liver fibrosis has not been well studied, particularly in human disease. Here, we show that the thickness, ECM content and organisation, cellular composition, and mechanical properties of the human capsule change significantly in cirrhosis, suggesting that the capsule is an active site of human liver disease.

The capsule is part of the visceral fascia[1]; our data are consistent with published data showing that fascia has a role in disease pathogenesis, and that changes in elastic fibres, HA, and collagen, with associated fascial thickening, can lead to abnormal mechanics and function.[23–28] Although strong similarities exist, exact changes in ECM composition at different sites of fascia are site specific.

The relationship between parenchymal and capsular pathology is still unclear. In mice, it has been shown that mesothelial cells and capsular fibroblasts migrate from the capsule to the liver parenchyma and contribute to the pool of activated myofibroblasts.[10,11] This and the fact that the capsule is continuous with the ECM surrounding the portal triad and vessels make a link very likely. Here, we show a correlation between capsular thickness and parenchymal fibrosis, specifically the thickness of collagen surrounding portal tracts, a hallmark of advancing disease and portal hypertension. However, a lack of correlation with parenchymal CD31 and angiogenesis suggests a more complex relationship. Unfortunately, we did not have access to patient clinical data beyond fibrosis stage and liver disease aetiology,

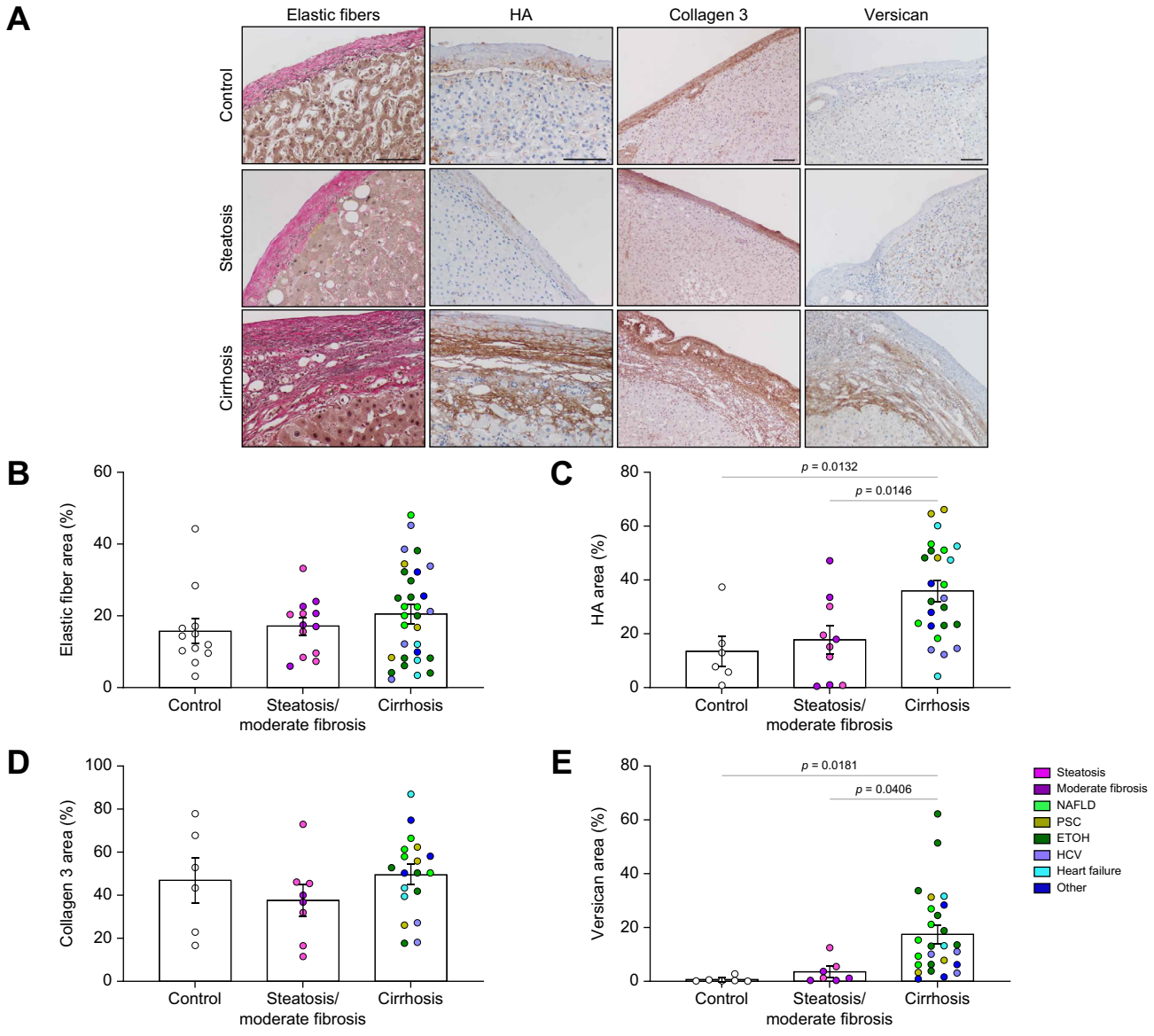

Fig. 5. Deposition of key matrix components in the liver capsule. (A) Representative imaging of elastic fibre (Van Gieson stain; black), HA (brown), collagen 3 (brown), and versican (brown) staining from control, steatotic or cirrhotic samples (NAFLD in this example). (B) Quantification of elastic fibre percentage area. N = 12–31. (C) Quantification of HA percentage area. N = 6–26. (D) Quantification of collagen 3 percentage area. N = 6–19. (E) Quantification of versican percentage area. N = 7–26. Data were analysed by one-way ANOVA and are shown as mean ± SEM. Scale bars: 100 μm. ETOH, ethanol-induced liver disease; HA, hyaluronic acid; NAFLD, non-alcoholic fatty liver disease; PSC, primary sclerosing cholangitis.

limiting our analysis of the relationship between histological and mechanical changes and clinical outcome. Additionally, current technologies are not yet reliable enough for mechanical measurements of the capsule: reverberation artefacts caused by changes in the subscapular area and heterogeneity of the diseased capsule make accurate measurements difficult.

There was a particularly significant increase in deposition of HA in the cirrhotic capsule. This is consistent with increases in HA observed in the parenchyma and, notably, in the serum of patients with cirrhosis, in whom it is used as a biomarker for diagnosis.[29,30] Increases in HA in the liver result from both increased production and decreased clearance by damaged liver sinusoidal endothelial cells (SECs).[31] In the capsule, where the number of fibroblasts is increased and there are few SECs, increased production is most likely, although decreased clearance from SECs adjacent to the capsule could also contribute. The increase in HA would likely have both physical and biochemical consequences. HA undergoes swelling, creating and occupying space within a tissue, allowing for better cell migration and collagen deposition[32–34]; indeed, we observed HA protruding between pairs of hepatocytes at the interface of the newly deposited capsule and parenchyma. In liver fibrosis, HA mediates hepatic stellate cell myofibroblastic activation, angiogenesis, and BEC proliferation.[35–37] Colocalisation of these in the lower capsule suggests a similar effect on cells within the capsule. Versican, an HA-binding proteoglycan found primarily in the cirrhotic capsule, is also involved in collagen fibrillogenesis, cell adhesion and migration, and signalling.[38,39] It is a likely

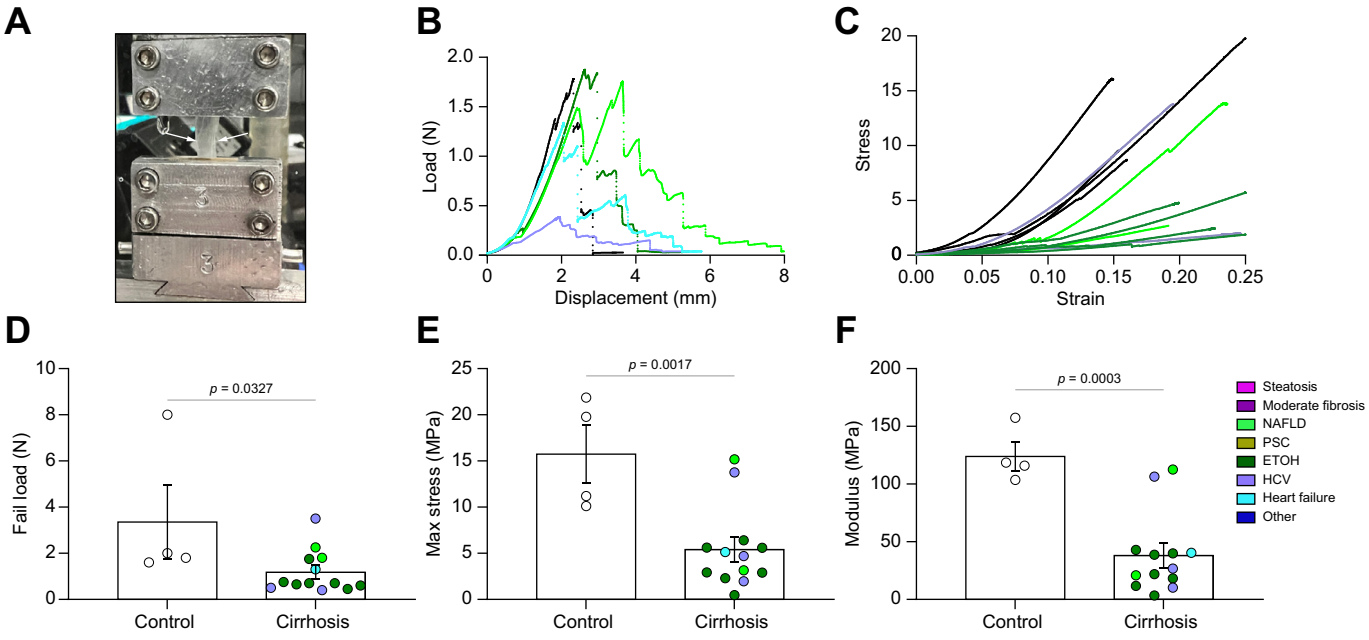

Fig. 6. Capsules from patients with cirrhosis are less stiff than those from control patients. (A) Capsule (between white arrows) gripped in place during a tensile test. (B) Representative force–displacement curves. (C) Representative stress–strain curves. (D) Ultimate loads at tissue failure. (E) Calculated maximum stresses at tissue failure. (F) Calculated moduli at high strain. Data were analysed with an unpaired two-way Student's *t* test and are shown as mean ± SEM. N = 4–13. ETOH, ethanol-induced liver disease; NAFLD, non-alcoholic fatty liver disease; PSC, primary sclerosing cholangitis.

contributor to the change in the collagen network organisation observed within the capsule, given that it is known to bind collagen fibres directly and to drive collagen bundle organisation.[38,40] Versican can also induce a profibrotic phenotype in capsular fibroblasts and adjacent hepatic stellate cells.[39,41]

Our data show that the majority of changes in the capsule in fibrosis occur in patients with end-stage cirrhosis, suggesting that capsule changes are secondary to parenchymal disease. The late manifestations of capsular disease might also reflect the unique subpopulations of both macrophages and fibroblasts residing in the capsule. Capsular macrophages are believed to provide immunosurveillance against pathogens within the peritoneum and could protect against early disease.[8,42] Capsular fibroblasts also highly express the transcription factor Odd-skipped related transcription factor 1 (Osr1),[8] which is protective against inflammation and early fibrosis in a fatty liver disease mouse model.[43] Thus, both capsular fibroblasts and macrophages might have a basal anti-inflammatory phenotype.

Mesothelial cells have previously been shown in rodents to migrate into the liver parenchyma and differentiate into myofibroblasts participating in collagen deposition.[11] No mesothelial cells could be observed within the capsule or in the 'active zone' in our samples, suggesting that that transmigration of these cells in human disease is limited. However, mesothelial cells were not found consistently on the surface of samples, and appeared to have detached during handling of the tissue, making any comment on this process difficult.

Mechanical testing of patient capsules showed that liver cirrhosis leads to important functional changes in the capsule. In contrast to the rest of the liver, which stiffens in fibrosis and cirrhosis, capsules from cirrhotic livers were less resistant to mechanical loads compared with controls.[12,13] We speculate that this is protective and a compensatory mechanism in the context of pathologically high intrahepatic pressures, preventing the further increases in pressure that would occur with a more rigid capsule. The key difference in mechanics between the liver and the capsule in disease reflects the starting mechanical properties and composition of the tissue. The bulk of the liver is highly cellular, with limited matrix, and is relatively soft. In fibrosis, the matrix is cross-linked and becomes highly organised within the tissue, leading to increased overall rigidity. By contrast, we show here that the normal liver capsule is a matrix-rich tissue organised into a two-fibre family pattern, consistent with measurements showing it to be a relatively stiff tissue.[18] In fibrosis, key matrix properties, such as crimping and organisation, are altered, and this likely leads to the observed softening. The crimp found in collagen fibres allows for gradual fibre extension during tensile testing, consistent with the biphasic response observed in normal liver capsule, similar to that observed in tendon.[44] Collagen crimping is reduced in cirrhotic capsules, leading to decreased elasticity and increased brittleness, as observed by the lower fail load of the cirrhotic capsule compared with the control. Organisation of the collagen network drives tissue stiffness: a disorganised network is less stiff than a network in which fibres are well aligned.[18,45] Previous studies found the normal capsule to have a modulus between 27.7 MPa[21] and 48.7 Mpa.[22] The control samples we report here had a modulus of 123.9 MPa, which, although slightly higher, is a similar order of magnitude. There are two factors that could contribute to the higher modulus we observed. The two previously published studies were carried out on livers from cadavers in which degradation of the tissues is likely to have started, leading to reduced tissue integrity. When comparing fresh (tested within 5 days of death) and frozen tissue, the fresh tissue appeared to have a relative decrease in modulus (16.9 MPa *vs.* 27.7 MPa).[21] Second, the controls used in our study were from uninvolved tissue adjacent to colon cancer metastases and, although histology of these sections was normal, there might have been underlying mechanical changes.

Conclusions

Our data support viewing the liver capsule, a part of the interstitium and visceral fascia, as an active, albeit secondary, site of liver disease. The secondary nature of changes in the capsule limits their clinical value as predictive markers for progression, although they could be useful in disease staging. We note that cirrhosis leads to significant mechanical changes, resulting in a more compliant capsule that might serve as a limited compensatory mechanism to reduce portal hypertension in cirrhosis. The capsule should be considered when developing diagnostic and therapeutic approaches for liver fibrosis and cirrhosis.

Abbreviations

BEC, biliary epithelial cell; ECM, extracellular matrix; EHBD, extrahepatic bile duct; ETOH, ethanol-induced liver disease; HA, hyaluronic acid/hyaluronan; IRB, institutional review board; NAFLD, non-alcoholic fatty liver disease; Osr1, Odd-skipped related transcription factor 1; PSC, primary sclerosing cholangitis; SEC, sinusoidal endothelial cell; SHG, second harmonic generation; SMA, smooth muscle actin.

Financial support

This work was supported by the Center for Engineering MechanoBiology, an NSF Science and Technology Center, under grant agreement CMMI: 15-48571, and by NIH/NIBIB R01 EB017753 (to RGW).

Conflicts of interest

The authors declare no conflict of interest.

Please refer to the accompanying ICMJE disclosure forms for further details.

Authors' contributions

Study concept and design: JL, CF; Acquisition, analysis, and interpretation of data: JL, CF, AL, CSF, MH; Drafting of the manuscript: JL, CF; Provided material support and contributed to data interpretation: NDT, EEF, MG; Conceived ideas and designed the research, provided critical revision of the manuscript, obtained funding, and supervised the study: RGW, CS.

Data availability statement

The authors confirm that the data supporting the findings of this study are available within the article and/or its supplementary materials.

Acknowledgements

We would like to acknowledge our gratitude to the Molecular Pathology and Imaging Core of the UPenn NIDDK Center for Molecular Studies in Digestive and Liver Diseases (NIH P30 DK050306), Gordon Ruthel and the Penn Vet imaging core (NIH S10 OD021633-01), and the Perelman School of Medicine Cell and Developmental Biology Microscopy Core, for their assistance throughout this project.

Supplementary data

Supplementary data to this article can be found online at https://doi.org/10.1016/j.jhepr.2023.100760.

References

Author names in bold designate shared co-first authorship

[1] Stecco C, Sfriso MM, Porzionato A, Rambaldo A, Albertin G, Macchi V, et al. Microscopic anatomy of the visceral fasciae. J Anat 2017;231:121–128.
[2] Federative Committee on Anatomical Terminology. Terminologia anatomica : international anatomical terminology. New York: Thieme; 1998.
[3] Benias PC, Wells RG, Sackey-Aboagye B, Klavan H, Reidy J, Buonocore D, et al. Structure and distribution of an unrecognized interstitium in human tissues. Sci Rep 2018;8:4947.
[4] Hayashi S, Murakami G, Ohtsuka A, Itoh M, Nakano T, Fukuzawa Y. Connective tissue configuration in the human liver hilar region with special reference to the liver capsule and vascular sheath. J Hepatobiliary Pancreat Surg 2008;15:640–647.
[5] Wang J, Kubes P. A reservoir of mature cavity macrophages that can rapidly invade visceral organs to affect tissue repair. Cell 2016;165:668–678.
[6] Sinturel F, Gerber A, Mauvoisin D, Wang J, Gatfield D, Stubblefield JJ, et al. Diurnal oscillations in liver mass and cell size accompany ribosome assembly cycles. Cell 2017;169:651–663.
[7] Leung NW, Farrant P, Peters TJ. Liver volume measurement by ultrasonography in normal subjects and alcoholic patients. J Hepatol 1986;2(2):157–164.
[8] **Guilliams M**, **Bonnardel J**, **Haest B**, **Vanderborght B**, Wagner C, Remmerie A, et al. Spatial proteogenomics reveals distinct and evolutionarily conserved hepatic macrophage niches. Cell 2022;185:379–396.e38.
[9] Xu S, Kang CH, Gou X, Peng Q, Yan J, Zhuo S, et al. Quantification of liver fibrosis via second harmonic imaging of the Glisson's capsule from liver surface. J Biophotonics 2016;9:351–363.
[10] Balog S, Li Y, Ogawa T, Miki T, Saito T, French SW, et al. Development of capsular fibrosis beneath the liver surface in humans and mice. Hepatology 2020;71:291–305.
[11] Li Y, Wang J, Asahina K. Mesothelial cells give rise to hepatic stellate cells and myofibroblasts via mesothelial-mesenchymal transition in liver injury. Proc Natl Acad Sci U S A 2013;110:2324–2329.
[12] Georges PC, Hui JJ, Gombos Z, McCormick ME, Wang AY, Uemura M, et al. Increased stiffness of the rat liver precedes matrix deposition: implications for fibrosis. Am J Physiol Gastrointest Liver Physiol 2007;293:G1147–G1154.
[13] Yeh WC, Li PC, Jeng YM, Hsu HC, Kuo PL, Li ML, et al. Elastic modulus measurements of human liver and correlation with pathology. Ultrasound Med Biol 2002;28:467–474.
[14] Lee JW, Kim S, Kwack SW, Kim CW, Moon TY, Lee SH, et al. Hepatic capsular and subcapsular pathologic conditions: demonstration with CT and MR imaging. Radiographics 2008;28:1307–1323.
[15] Williams RM, Zipfel WR, Webb WW. Interpreting second-harmonic generation images of collagen I fibrils. Biophys J 2005;88:1377–1386.
[16] Favata M, Beredjiklian PK, Zgonis MH, Beason DP, Crombleholme TM, Jawad AF, et al. Regenerative properties of fetal sheep tendon are not adversely affected by transplantation into an adult environment. J Orthop Res 2006;24:2124–2132.
[17] Sharabi M. Structural mechanisms in soft fibrous tissues: a review. Front Mater 2021;8:793647.
[18] Lee W, Moghaddam AO, Lin Z, McFarlin BL, Wagoner Johnson AJ, Toussaint KC. Quantitative classification of 3D collagen fiber organization from volumetric images. IEEE Trans Med Imaging 2020;39:4425–4435.
[19] Witte M, Jaspers S, Wenck H, Rübhausen M, Fischer F. General method for classification of fiber families in fiber-reinforced materials: application to in-vivo human skin images. Sci Rep 2020;10:10888.
[20] Volk SW, Wang Y, Mauldin EA, Liechty KW, Adams SL. Diminished type III collagen promotes myofibroblast differentiation and increases scar deposition in cutaneous wound healing. Cells Tissues Organs 2011;194:25–37.
[21] Brunon A, Bruyère-Garnier K, Coret M. Mechanical characterization of liver capsule through uniaxial quasi-static tensile tests until failure. J Biomech 2010;43:2221–2227.
[22] Jayyosi C, Coret M, Bruyère-Garnier K. Imaging of the human Glisson's capsule by two-photon excitation microscopy and mechanical characterisation by uniaxial tensile tests. Comput Methods Biomech Biomed Eng 2013;16(Suppl 1):282–283.
[23] Wilke J, Macchi V, De Caro R, Stecco C. Fascia thickness, aging and flexibility: is there an association? J Anat 2019;234:43–49.
[24] **Bertoldo D**, **Pirri C**, Roviaro B, Stecco L, Day JA, Fede C, et al. Pilot study of sacroiliac joint dysfunction treated with a single session of fascial manipulation. Medicina (Kaunas) 2021;57:691.
[25] Casato G, Stecco C, Busin R. Role of fasciae in nonspecific low back pain. Eur J Transl Myol 2019;29:8330.
[26] Fantoni I, Biz C, Fan C, Pirri C, Fede C, Petrelli L, et al. Fascia lata alterations in hip osteoarthritis: an observational cross-sectional study. Life (Basel) 2021;11:1136.

[27] Ozdogan M, Yildiz F, Gurer A, Orhun S, Kulacoglu H, Aydin R. Changes in collagen and elastic fiber contents of the skin, rectus sheath, transversalis fascia and peritoneum in primary inguinal hernia patients. Bratisl Lek Listy 2006;107:235–238.
[28] Fede C, Pirri C, Fan C, Albertin G, Porzionato A, Macchi V, et al. Sensitivity of the fasciae to sex hormone levels: modulation of collagen-I, collagen-III and fibrillin production. PLoS One 2019;14:e0223195.
[29] Gudowska M, Gruszewska E, Panasiuk A, Cylwik B, Flisiak R, Świderska M, et al. Hyaluronic acid concentration in liver diseases. Clin Exp Med 2016;16:523–528.
[30] Orasan OH, Ciulei G, Cozma A, Sava M, Dumitrascu DL. Hyaluronic acid as a biomarker of fibrosis in chronic liver diseases of different etiologies. Clujul Med 2016;89:24–31.
[31] Reinders ME, van Wagensveld BA, van Gulik TM, Frederiks WM, Chamuleau RA, Endert E, et al. Hyaluronic acid uptake in the assessment of sinusoidal endothelial cell damage after cold storage and normothermic reperfusion of rat livers. Transpl Int 1996;9:446–453.
[32] Lai VK, Nedrelow DS, Lake SP, Kim B, Weiss EM, Tranquillo RT, et al. Swelling of collagen-hyaluronic acid co-gels: an in vitro residual stress model. Ann Biomed Eng 2016;44:2984–2993.
[33] Yang YL, Sun C, Wilhelm ME, Fox LJ, Zhu J, Kaufman LJ. Influence of chondroitin sulfate and hyaluronic acid on structure, mechanical properties, and glioma invasion of collagen I gels. Biomaterials 2011;32:7932–7940.
[34] Solis MA, Chen YH, Wong TY, Bittencourt VZ, Lin YC, Huang LL. Hyaluronan regulates cell behavior: a potential niche matrix for stem cells. Biochem Res Int 2012;2012:346972.
[35] Yang YM, Noureddin M, Liu C, Ohashi K, Kim SY, Ramnath D, et al. Hyaluronan synthase 2-mediated hyaluronan production mediates Notch1 activation and liver fibrosis. Sci Transl Med 2019;11:eaat9284.
[36] Ghose S, Biswas S, Datta K, Tyagi RK. Dynamic Hyaluronan drives liver endothelial cells towards angiogenesis. BMC Cancer 2018;18:648.
[37] He Y, Wu GD, Sadahiro T, Noh SI, Wang H, Talavera D, et al. Interaction of CD44 and hyaluronic acid enhances biliary epithelial proliferation in cholestatic livers. Am J Physiol Gastrointest Liver Physiol 2008;295:G305–G312.
[38] Chen D, Smith LR, Khandekar G, Patel P, Yu CK, Zhang K, et al. Distinct effects of different matrix proteoglycans on collagen fibrillogenesis and cell-mediated collagen reorganization. Sci Rep 2020;10:19065.
[39] Wight TN, Kang I, Evanko SP, Harten IA, Chang MY, Pearce OMT, et al. Versican–a critical extracellular matrix regulator of immunity and inflammation. Front Immunol 2020;11:512.
[40] Chen D, Du Y, Llewellyn J, Bonna A, Zuo B, Janmey PA, et al. Versican binds collagen via its G3 domain and regulates the organization and mechanics of collagenous matrices. bioRxiv 2022:2022. 03.27.485990.
[41] Bukong TN, Maurice SB, Chahal B, Schaeffer DF, Winwood PJ. Versican: a novel modulator of hepatic fibrosis. Lab Invest 2016;96:361–374.
[42] Sierro F, Evrard M, Rizzetto S, Melino M, Mitchell AJ, Florido M, et al. A liver capsular network of monocyte-derived macrophages restricts hepatic dissemination of intraperitoneal bacteria by neutrophil recruitment. Immunity 2017;47:374–388.
[43] **Zhou Y**, **Liu Z**, Lynch EC, He L, Cheng H, Liu L, et al. Osr1 regulates hepatic inflammation and cell survival in the progression of non-alcoholic fatty liver disease. Lab Invest 2021;101:477–489.
[44] Freed AD, Doehring TC. Elastic model for crimped collagen fibrils. J Biomech Eng 2005;127:587–593.
[45] Gasser TC, Ogden RW, Holzapfel GA. Hyperelastic modelling of arterial layers with distributed collagen fibre orientations. J R Soc Interf 2006;3:15–35.

Journal of Hepatology, Volume *5*

Supplemental information

Glisson's capsule matrix structure and function is altered in patients with cirrhosis irrespective of aetiology

Jessica Llewellyn, Caterina Fede, Abigail E. Loneker, Chet S. Friday, Michael W. Hast, Neil D. Theise, Emma E. Furth, Maria Guido, Carla Stecco, and Rebecca G. Wells

Supplementary data

Glisson's capsule matrix structure and function is altered in patients with cirrhosis irrespective of etiology

Jessica Llewellyn, Caterina Fede, Abigail E. Loneker, Chet S. Friday, Michael W. Hast, Neil D. Theise, Emma E. Furth, Maria Guido, Carla Stecco, Rebecca G. Wells

Table of Contents:

Supplementary Methods

Histology & Staining:

For diaminobenzidine (DAB) labelling, sections were incubated in 3% H_2O_2 to quench endogenous peroxidases (Sigma Aldrich, Rockville, MA), and then blocked for avidin/biotin (Vector Laboratories, Newark, CA) followed by StartingBlock™ T20/phosphate buffered saline (PBS) Blocking Buffer (Thermo Fisher Scientific, Waltham, MA). Samples were incubated in primary antibodies (staining buffer-0.2% Triton X-100, 0.1% bovine serum albumin, in PBS) overnight at 4°C. After washing in PBS, samples were washed and incubated with appropriate biotinylated secondary antibodies (Vector Laboratories) for 1 h at room temperature. Hyaluronic acid/hyaluronan (HA) was stained overnight using biotinylated HA binding protein (Millipore, Burlington, MA; 385911). All sections were washed and incubated with VECTASTAIN® ABC-HRP kit (Vector Laboratories). Staining was developed with a DAB substrate kit (Vector Laboratories). Elastic fibers were stained using an elastic stain kit (Sigma-Aldrich, HT25A-1KT) per the manufacturer's instructions. Sections were imaged by brightfield microscopy using a Nikon E600 and NIS-elements software (Nikon, Melville, NY).

For fluorescence staining, sections were blocked with StartingBlock™ T20/phosphate buffered saline (PBS) Blocking Buffer before incubation in primary antibodies (staining buffer) overnight at 4°C, followed by washing and incubation with fluorescent secondary antibody for 1 h at RT in the dark. Staining was imaged on a Zeiss Axio Observer 7 inverted microscope (Zeiss Axiocam 701 monochrome CMOS camera) and Zen blue software (Zeiss, White Plains, NY). All antibodies used are listed in Supplementary Table 1.

For picrosirius red staining, paraffin-embedded sections were dewaxed and rehydrated as above. Sections were then incubated in PSR stain (Poly Scientific R&D, Bay Shore, NY) for 1 h at RT. Sections were then quickly washed in acidified water (0.5% acetic acid in H_2O), and dehydrated in 3 washes of 100% ethanol before clearing in Xylene and mounting.

Image analysis

Thickness, percentage area and cell counting were analyzed using ImageJ (1). 3-5 images per liver were taken using the same parameters and analyzed using manually-determined regions of interest. Thickness was measured manually, with 5 measurements per image. Quantification of percentage area for DAB-stained slides was carried out using the deconvolution tool H DAB followed by thresholding. Percentage area of collagen in SHG cross-sections was also done using thresholding. Capsule areas were divided into two areas, the upper 70 μm and a lower layer (anything further than 70 μm from the

surface), using separate regions of interest. Cells were counted using the particle analysis tool. CD31 structures were counted manually using the count tool. Structures were defined as 2 or more clustered cells; some of these formed vessel-like structures.

Picro Sirius red staining was analyzed under polarized light with 6-10 images analyzed per sample. The PSR dye enhances the natural birefringence of the collagen when exposed to polarized light (2). PSR images were used to estimate a uniformity index of collagen fiber distribution, as previously described (3). This index calculates values between 1 (when the objects are distributed in a regular array) and 0 (when maximal clustering occurs). In order to apply this method, a subsampled binary image of the collagen pattern was obtained by extracting pixels corresponding to the points of a superimposed regular/systematic grid.

Crimping of collagen fibers was assessed on z stacks of SHG images. Depth and length were manually measured using the line tool in ImageJ. Approximately 20 fibers were measured in 3-8 images per sample. Orientation and alignment of collagen fibers were also assessed on SHG Z-stacks using a previously described method (4).

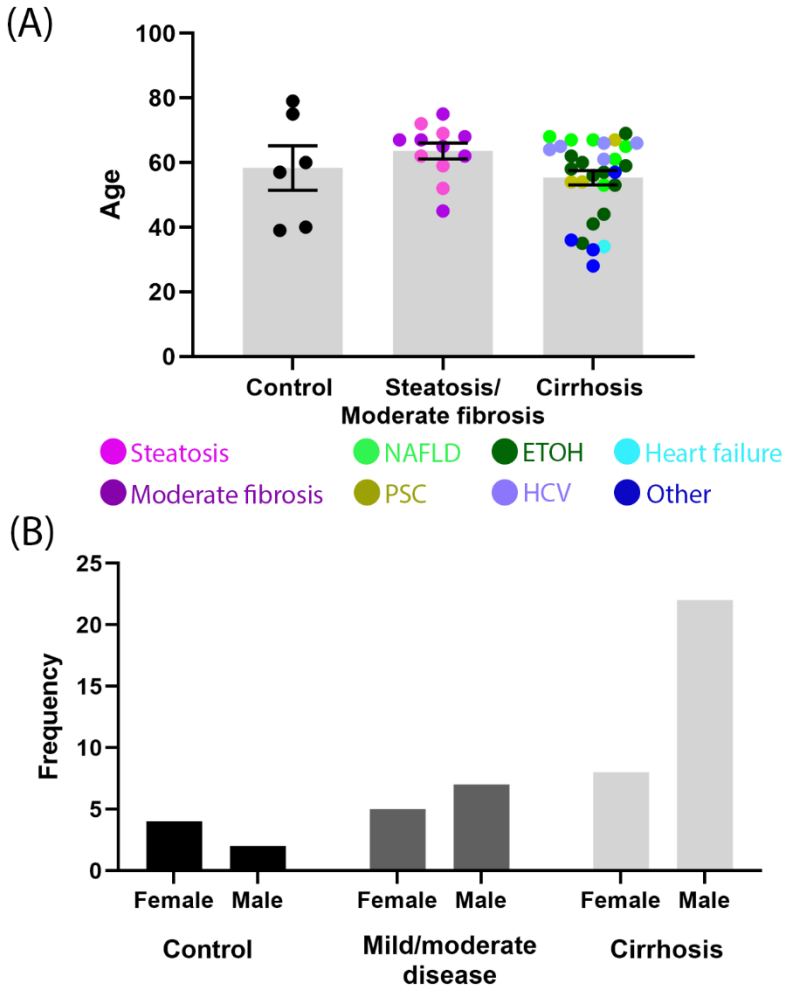

1. Sex and age of patient samples. (A) Patient ages for the control, steatosis/moderate fibrosis and cirrhotic samples used. (B) Sex distribution of patients for the control, steatosis/moderate fibrosis and cirrhotic samples used.

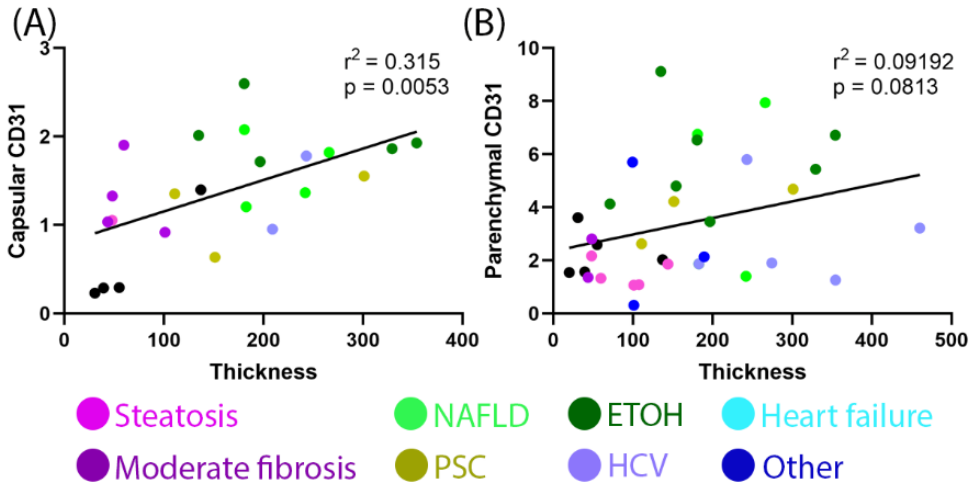

Fig. S2. Capsule thickness correlates with capsular CD31 but not parenchymal CD31. (A) Correlation between capsular thickness and capsular CD31 structures. (B) Correlation between capsular thickness and parenchymal CD31 percentage staining. Correlation analyzed by Pearson's correlation.

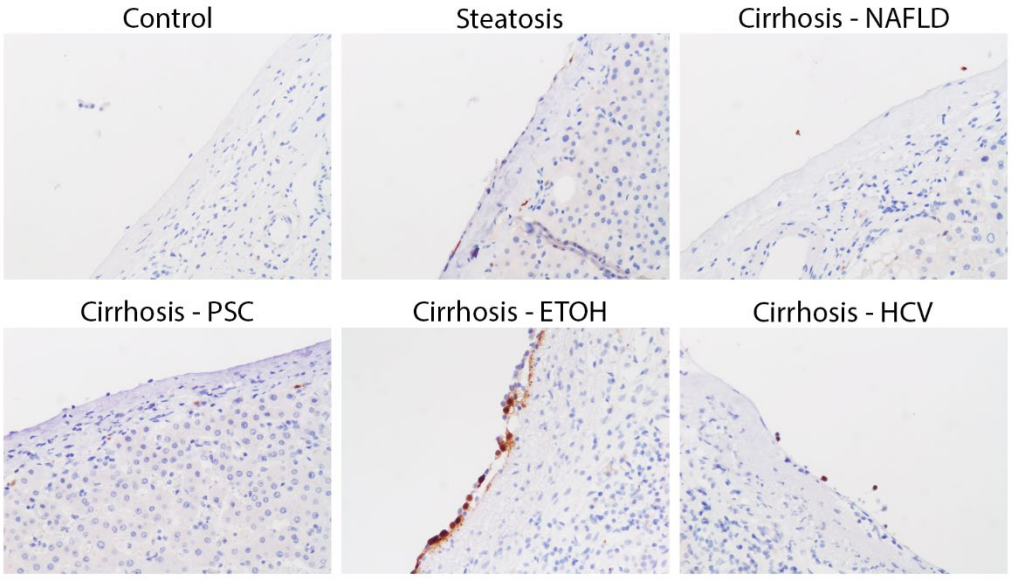

Fig. S3. Mesothelial cells are found sporadically on the capsule surface. Representative staining for calretinin in control and steatotic samples as well as cirrhotic samples of different etiologies.

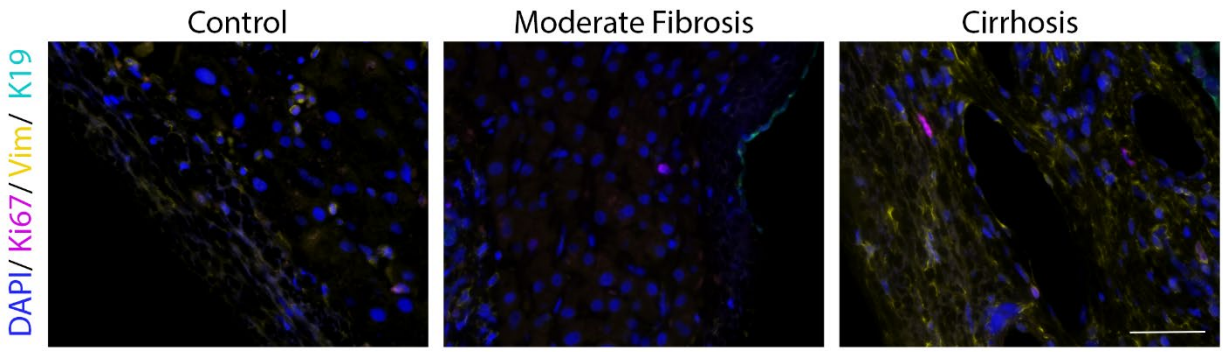

Fig. S4. Proliferation is unchanged in disease. Representative images of control, moderately fibrotic and cirrhotic samples (NAFLD in this example) stained for DAPI (nucleus; blue), Ki67 (proliferation, magenta), vimentin (fibroblasts; yellow), and K19 (BECs; cyan). Scale bars 50 μm.

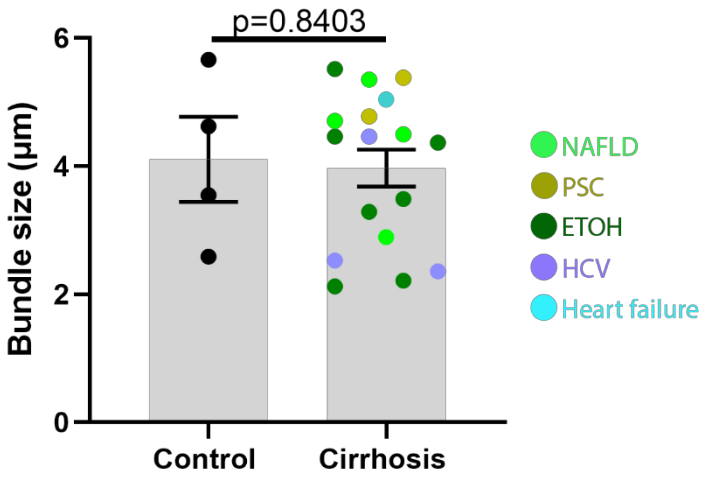

Fig. S5. Collagen bundling is unaffected by disease. Quantification of collagen bundle size. Data were analyzed with an unpaired two-tailed student t test and are shown as mean ± SEM. N=4-17

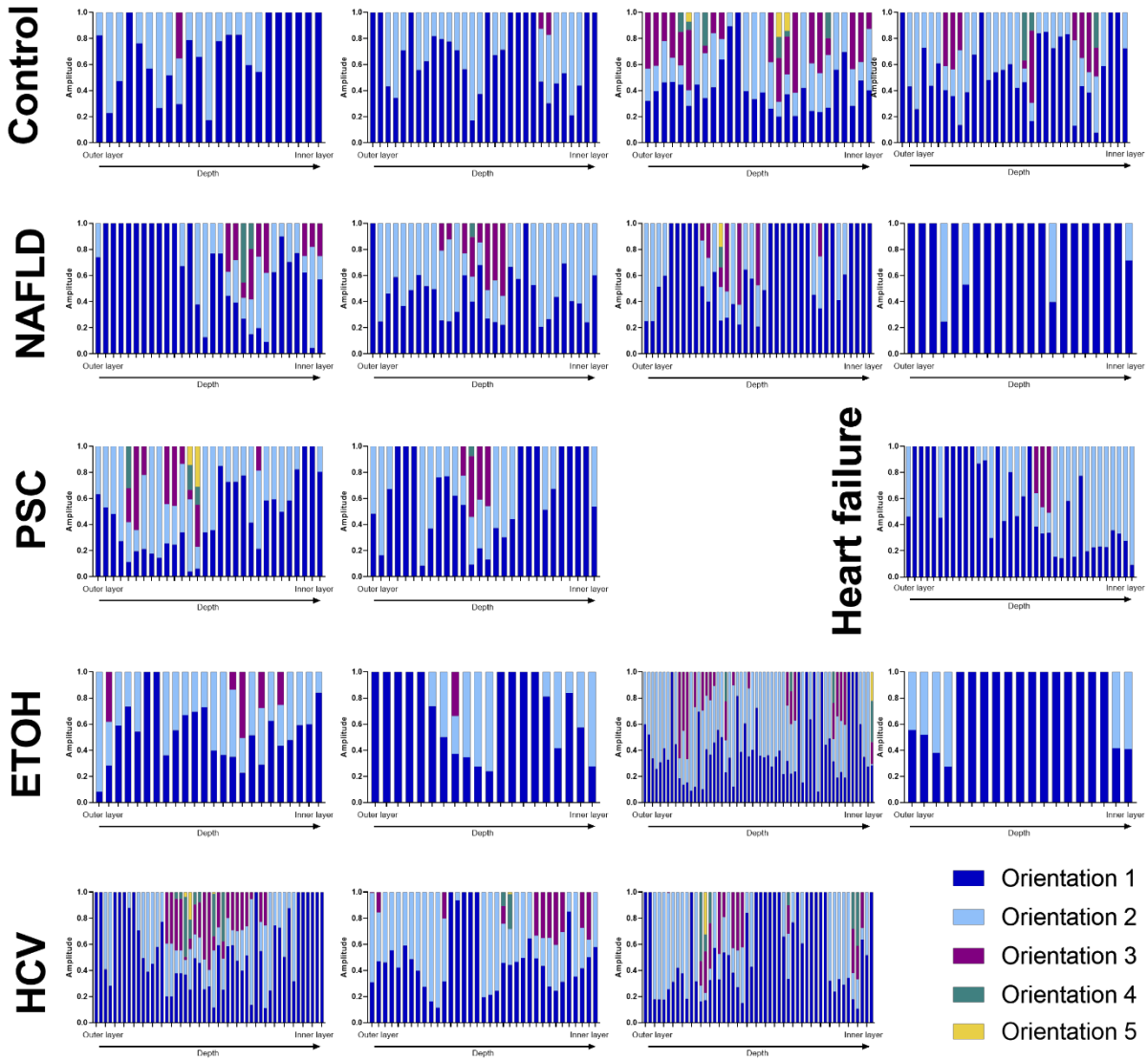

Fig. S6. Amplitude of collagen orientation families. Fibers from SHG z stacks placed into families of similar orientation for control and cirrhotic liver samples of different etiologies.

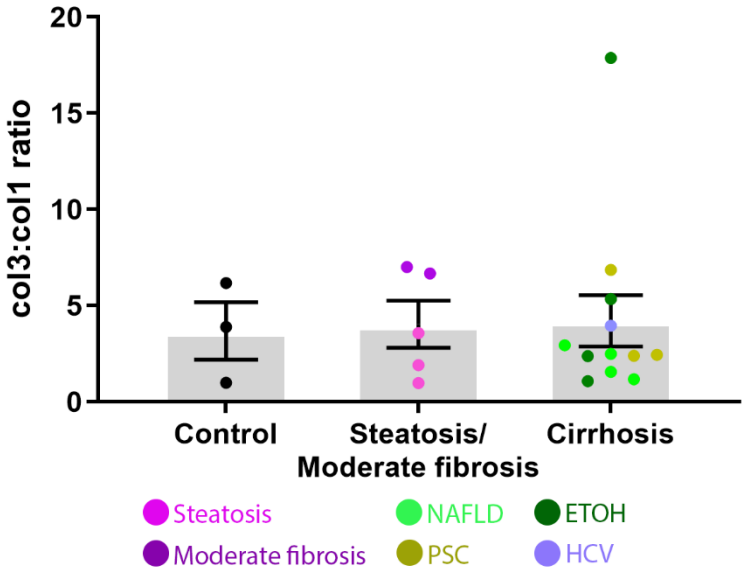

Fig. S7. Collagen 3 to collagen 1 ratio is unaltered in capsules in diseased livers. Quantification of collagen 3 to 1 ratio. Data were analyzed by one-way ANOVA and are shown as mean ± SEM. N=5-14.

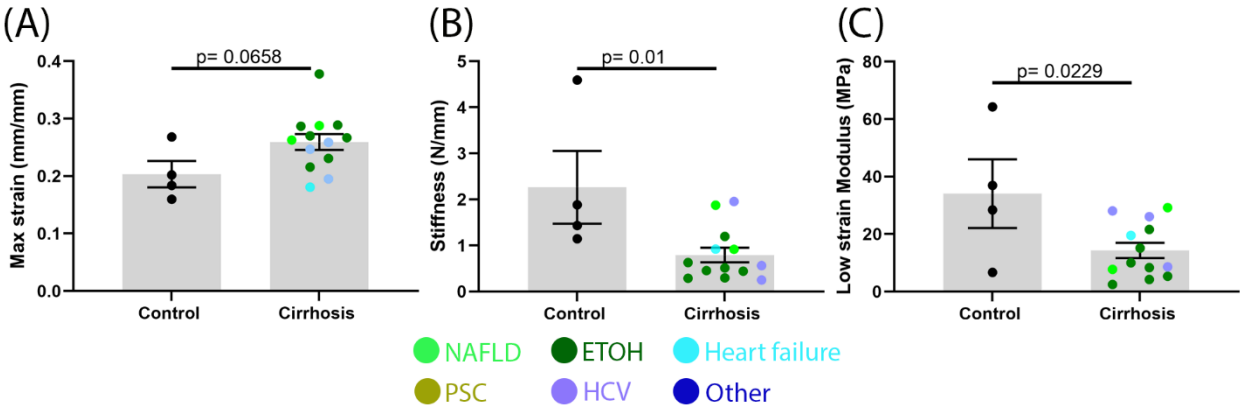

Fig. S8. Liver capsule mechanics are altered in cirrhotic patients. (A) Maximum strain at which tissue starts to fail. (B) Calculated stiffness. (C) Calculated moduli at low strain (approx. 4-6%). Data were analyzed with an unpaired two-way student t test and are shown as mean ± SEM. N=4-14.

Primary antibodies			
Antigen	**Species**	**Dilution**	**Source**
αSMA	Mouse	1:100	Sigma, A2547
Collagen 3	Goat	1:100	Southern Biotech ,1330-01
Cytokeratin 7 (K7)	Rabbit	1:200	Abcam, ab68459
Cytokeratin 19 (K19)	Mouse	1:200	Abcam, ab7754
Ki67	Rabbit	1:100	Abcam, ab16667
CD45	Rat	1:50	Novus, NB100-77417SS
Vimentin	Chicken	1:500	Novus, NB300 223
CD68	Mouse	1:100	Abcam, ab955
CD31	Rabbit	1:100	Novus, NB100-2284
Calretinin	Rabbit	1:100	Thermofisher, PA5-32287
Versican	Rabbit	1:200	Novus, NBP1-85432
Biotinylated anti-Rabbit	Donkey	1:200	Vector Laboratories, BA-1000
Biotinylated anti-Goat	Donkey	1:200	Vector Laboratories, BA-9500
Cy 2 anti-mouse	Donkey	1:500	Vector Laboratories ,715-225-150
Cy 3 anti-rabbit	Donkey	1:500	Vector Laboratories, 711-165-152
Cy3 anti-rat	Donkey	1:500	Vector Laboratories, 712-165-153
Cy5 anti-chicken	Donkey	1:500	Vector Laboratories, 703-605-155

Supplementary Table 1: Antibodies used

Supplementary References:

1. Schindelin J, Arganda-Carreras I, Frise E, Kaynig V, Longair M, Pietzsch T, et al. Fiji: an open-source platform for biological-image analysis. Nat Methods. 2012;9(7):676-82.
2. Montes GS, Junqueira LC. The use of the Picrosirius-polarization method for the study of the biopathology of collagen. Mem Inst Oswaldo Cruz. 1991;86 Suppl 3:1-11.
3. Guidolin D, Nico B, Crivellato E, Marzullo A, Vacca A, Ribatti D. Tumoral mast cells exhibit a common spatial distribution. Cancer Lett. 2009;273(1):80-5.
4. Witte M, Jaspers S, Wenck H, Rübhausen M, Fischer F. General method for classification of fiber families in fiber-reinforced materials: application to in-vivo human skin images. Sci Rep. 2020;10(1):10888.